Journal of Physics: Conference Series **1393** (2019) 012021 doi:10.1088/1742-6596/1393/1/012021

Temperature gradients in targets with high-intensity implantation and their influence on the characteristics of ion-modified layers

A I Ryabchikov[1], I V Lopatin[2], P S Ananin[1], G A Bleicher[1], A I Ivanova[1], T V Koval[1], G S Modebadze[1] and D O Sivin[1]

[1] National Research Tomsk Polytechnic University, 30 Lenin Ave., Tomsk, 634050, Russia
[2] Institute of High Current Electronics SB RAS, 2/3 Akademichesky Ave., Tomsk, 634055, Russia

E-mail: lopatin@opee.hcei.tsc.ru

Abstract. This paper is devoted to the study of the gradient temperature field dynamics and distribution in the metal targets irradiated with high-intensity beams of gas and metal ions. The investigations concerned ion implantation modes with the ion beam current density from several tens of mA·cm^{-2} up to A·cm^{-2} were investigated. The ion beam power was additionally varied due to the change of ion energy in the range from 0.6 to several keV and the pulse duty factor in the range of 0.2–0.8. The integral temperature of the target was measured with an electrically isolated thermocouple. To measure the dynamic change in the local temperature on the irradiated target a high-temperature pulse pyrometer KLEIBER 740-LO was used. The problem of temperature evolution and metal sample melting under the exposure of a high-intensity repetitively pulsed ion beam was solved numerically using the heat conduction equation written in cylindrical coordinates. Analysis of the experimental data obtained with the use of electrically isolated thermocouple, pulse pyrometer, and numerical simulation revealed the presence of significant gradient temperature fields both over the surface and along the depth of targets irradiated by high-intensity ion beams.

1. Introduction

Ion implantation as a method for modifying the surface and near-surface properties of materials has several advantages over other methods [1, 2]. Initially, the studies on ion implantation were carried out at ion current densities not exceeding tens and, only occasionally, hundreds of microamperes per square centimeter. At the same time, for the directional change in the properties of semiconductors, small irradiation fluences were required, usually not exceeding 10^{14} ions·cm^{-2}. In studies on the modification of microstructure and properties of metals and alloys, ion irradiation fluences of several orders of magnitude more (up to 10^{18} ions·cm^{-2}) were needed, which required the development and use of more high-current ion sources with ion current densities of up to several milliamperes per square centimeter [3–6]. Recently, high-intensity implantation of low-energy ions with ion current densities reaching several hundred milliamperes per square centimeter has been developed [7–10]. The peculiarity of high-intensity implantation is due to the significant energy characteristics of the ion beam. When the bias potential amplitude is 1.2 kV, the pulsed power density of the ion beam will

reach 0.3 kW·cm^{-2} [11]. Every second, an energy density of about 150 J·cm^{-2} is introduced into the surface layer of the material. Such densities of power and energy of the ion beam contribute to the rapid heating and increase in the irradiated target temperature. Moreover, if the target is thermally insulated, then its temperature increases very quickly, but the temperature gradient over the depth, on which the diffusion rate depends, decreases. When the target is mounted on a massive holder, the rate of the target heating by the ion beam decreases due to heat transfer from the target to the holder, but a significant temperature gradient is maintained over the target depth, and in the case of non-uniform ion current density and along the specimen surface. Since the specimen temperature, the temperature gradient over the surface and depth of the target largely determine the formation of concentration profiles of the implantable impurity distribution, the microstructure, and often the properties of materials, it is important to develop a method for measuring and calculating these parameters and verify it by comparing with various methods of experimental diagnostics.

This paper is devoted to analyzing the problems of correct measurement of the high-intensity ion beam parameters, dynamically changing temperature fields during high-intensity implantation, and to the developing numerical calculation models as temperature fields.

2. Features of the formation and measurement of high-intensity repetitively-pulsed ions

Repetitively-pulsed plasma-immersion ion beam formation in combination with ballistic focusing to achieve high ion current densities at relatively low accelerating voltages has a number of specific features that pose problems for both accurate measurement of the parameters of the ion beam itself and for accurate determination of, for example, temperature fields in the target, significantly affecting the mass transfer processes, changes in the microstructure and properties of ion-modified layers of various materials.

Let us consider successively various factors affecting the accuracy of measuring the main characteristics of the ion beam and irradiated target. First of all, the ion-beam formation is influenced by the presence of the extracting fine-structured mesh [12]. Plasma-immersion formation of an ion beam involves immersing a system into the plasma, including an extraction electrode and an electrode forming the drift space, with a repetitively-pulsed bias potential of negative polarity applied to them. The distribution of the electric field in the sheath layer near the grid electrode, immersed in the plasma, depends on the plasma density, the amplitude of the negative bias potential and the characteristic dimensions of the grid electrode cells.

The parameters of the ion beam formed in a repetitively-pulsed regime are significantly affected by the dynamics of a sheath layer formation. When a bias potential is applied to the grid electrode, due to the fast escape of the plasma electrons, a so-called “matrix layer” is formed near the grid electrode. In this "matrix layer", the ions are distributed uniformly over the width of the layer. Ion acceleration begins in the electric field of the sheath layer. In the initial state, the ions are in different places of the layer and, accelerating to the grid, they receive a different energy increment. As the ions accelerate, the density of ions in the layer redistributes and, as a result, the layer width increases. Dynamic change in the sheath layer characteristics leads to the formation, during some time, of an ion beam with a significant energy spread. Stabilization of the beam energy composition is achieved after the layer expansion to the size determined by the Child-Langmuir law [13]. According to experimental data, the stabilization time of the plasma ion-immersion boundary can be several hundred nanoseconds [14].

At small amplitudes of the bias potential, less than a kilovolt, the width of the sheath layer in the plasma, near the grid electrode, is comparable to the size of the grid cell. This leads to the fact that the plasma emission boundary ceases to be flat (in the approximation of a flat beam formation system) and, on the one hand, ion losses increase due to their contact with the grid, and secondly, the angular divergence of the ion flux increases, which worsens the conditions of the ion beam ballistic focusing. Thus, the formation of high-intensity ion beams at low bias potentials becomes problematic.

Taking into account the limitations in reducing the ion energy, it should be borne in mind that during high-intensity implantation with ion current densities of tens and hundreds of milliamperes per square centimeter, the fluences of ion irradiation, defined as $F = (j_i f \tau t)/Ze$, where j_i – ion current

density, f – pulse frequency, τ – pulse duration, Z – average ion charge state, e – elementary charge, t – ion irradiation time, will be very significant. For example, if the ion current density is 0.25 A·cm^{-2}, the duty factor of the bias potential is 0.5 and the target is irradiated for an hour, the ion irradiation fluence will be 2.25×10^{21} ions·cm^{-2}. Such ultrahigh fluences will lead to significant ionic sputtering of the irradiated target surface. Ion sputtering introduces two negative points. With ultrahigh irradiation fluences, the thickness of the surface sprayed layer of the target reaches several hundred micrometers. This significantly changes the surface morphology [15]. In addition, the sputtering of the surface layer of the target is accompanied by the spraying of a previously implanted impurity. For example, in [15], as a result of high-intensity implantation of nitrogen ions into 420 steel for one hour, the implanted impurity was detected at depths exceeding 90 μm. At the same time, the depth of the sprayed layer reached 180 microns. Thus, the total depth of radiation-stimulated diffusion of nitrogen atoms exceeded 270 μm. This means that it is possible to hope for the formation of wider ion-doped layers during high-intensity implantation of ions with energies providing a slight sputtering of the surface.

The characteristics of the ion beam current are significantly affected by dynamically changing conditions for neutralizing the space charge of the beam when it is transported in the initially equipotential space. The neutralization conditions, in turn, depend on the pre-filling of the drift space with plasma, the possibility of producing gas-discharge plasma, the degree of compression of the ion beam in the ballistic focusing process [16]. The manifestation of another feature depends on the pulse duration and amplitude of the bias potential. As shown in [17], at pulse durations of a bias potential of several tens of microseconds, the effect of disrupting the transport of a high-intensity ion beam may appear due to problems of space ion beam charge compensation due to the escape of plasma electrons into the high-voltage sheath layer through the grid electrode.

Taking into account the presence of a complex of problems, the determination of the energy parameters of a repetitively-pulsed ion beam using current and bias oscillograms will have a significant error.

For greater accuracy in measuring the ion beam energy characteristics, it is advisable to use calorimetric methods. However, in this case it is necessary to take into account a number of features associated with a high intensity of the ion beam. At ion current densities of several hundred milliamperes per square centimeter with an ion energy of about a kiloelectronvolt, the power density in the beam will be several hundred watts per square centimeter. At such power densities of the ion beam, the dynamic effects of heating the target and the temperature field gradients both in thickness and on the surface of the irradiated target become significant.

3. Numerical simulation of the temperature evolution of the specimen under high-intensity ion irradiation

To study the temperature evolution of a metal specimen under the action of a high-intensity repetitively-pulsed ion beam, a numerical model was developed using the heat equation written in cylindrical coordinates.

The computational domain of the problem is shown in figure 1. Here, a metal specimen in the form of a disk with radius R_1 and thickness h_1 is located on a holder in the form of a thin plate-disk with radius R_2 and thickness h_2. Since the distribution of the current density in the beam cross section and irradiated products have azimuthal symmetry, it was used to write the heat equation and solve the problem.

The mathematical formulation of the problem, taking into account the cost of heat for melting the elements of the irradiated composition, has the following form.

$$\frac{\partial E(z,r,t)}{\partial t}=\lambda(z)\frac{1}{r}\frac{\partial T(z,r,t)}{\partial r}+\lambda(z)\frac{\partial^2 T(z,r,t)}{\partial r^2}+\frac{\partial}{\partial z}\left(\lambda(z)\frac{\partial T(z,r,t)}{\partial z}\right) \quad (1)$$

Here $E(z,r,t)$ and $T(z,r,t)$ – space-time functions describing the distribution of the thermal component of the internal energy and temperature in the irradiated composition, and

$$T(z,r,t)=\begin{cases} E\ (\mathrm{z,r,t})/c(z)\rho(z), & E(z,r,t)\ \le E_m(\mathrm{z}), \\ T_m(\mathrm{z}), & E_m(z)<E\ (z,r,t)\le E_m(z)+q_m(z)\rho(z), \\ T_m(z)+(E(z,r,t)-(E_m(z)+q_m(z)\rho(z)))/c(z)\rho(z), & \\ & E(z,r,t)>E_m(z)+q_m(z)\rho(z). \end{cases} \quad (2)$$

Here λ, *c,* ρ – respectively, thermal conductivity coefficient, specific heat capacity and density of the irradiated substance; T_m and q_m – temperature and specific heat of melting; $E_m = T_m c\rho$. Depending on *z*, the thermal and physical characteristics of either the specimen or the holder are accepted.

Writing the thermal conductivity equation in the form (1), where *E* and *T* are related by relations (2), allows to take into account the cost of heat for melting in the calculations.

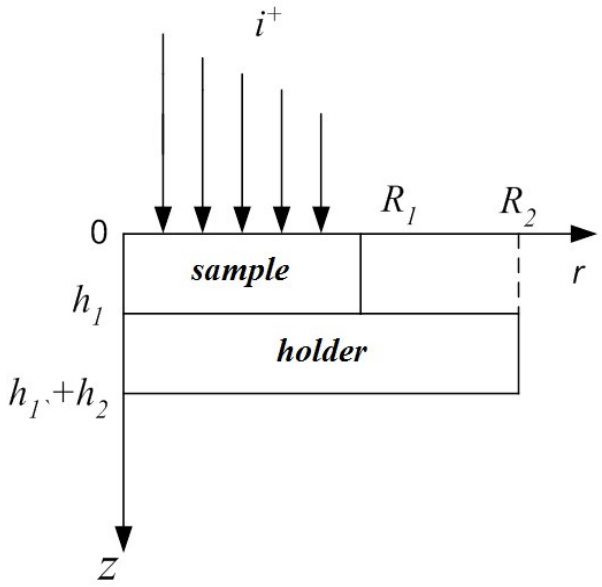

Figure 1. Computational domain: R_1 and R_2 – radii of the specimen and holder, h_1 and h_2 – thicknesses of the specimen and holder.

Initial conditions:

$$T(z,r)=T_0,\ E(z,r)=T_0c(z)\rho(z).$$

Boundary conditions on the irradiated surfaces of the specimen and holder:

$$\lambda(z)\frac{\partial T}{\partial z}\bigg|_{\substack{z=0,\\ 0\le r\le R_1}} = \lambda(z)\frac{\partial T}{\partial z}\bigg|_{\substack{z=h_1,\\ R_1<r\le R_2}} = -q(r)+\varepsilon_p(T^4-T_{ch}^4).$$

Here, $q(r)$ – ion beam power density averaged over the period, T_{ch} – wall temperature of the vacuum chamber, ε_p – reduced power of the surface blackness (specimen or holder), $\varepsilon_p = 1/((1/\varepsilon)+(1/\varepsilon_{ch}-1))$, where ε – surface blackness degree (specimen or holder), ε_{ch} – vacuum chamber blackness degree. In calculations T_{ch} = 300 K, ε_{ch} = 1.

On the remaining open surfaces of the composition, heat sinks due to thermal radiation are specified, on the axis *r*=0

$$\lambda(z)\frac{\partial T}{\partial r}\bigg|_{r=0} = 0 \cdot$$

An ideal thermally conductive contact was assumed in the contact area between the specimen and the holder.

The beam energy consumption for sputtering was not taken into account, since it is negligible compared with the beam power and thermal radiation. Evaporation was also not taken into account, since the purpose of the research was to use such irradiation regimes in which noticeable evaporation should not develop.

The power density function over the ion beam cross section radius q (r) was determined from experimental data on the current density and ion energy. Its change during the period was not taken into account, since the beam has a rather high pulse repetition rate ($f \sim 10^5$ imp.·s^{-1}). The calculations showed that the temperature variations during a single pulse of the ion beam impact amount to not more than 1 K.

Numerical calculations were carried out for the case of irradiation of a specimen of 5140 steel with a radius of 10 mm and a thickness of 4 mm, installed in the center of a holding plate made of stainless steel 12X18H10T with a radius of 30 mm and a thickness of 3 mm.

The formation of deep ion-modified layers of 5140 steel was carried out using a high-intensity repetitively-pulsed nitrogen ion beam with a pulsed current density from 1250 to 2800 A·m^{-2}, with a bias potential pulse duration of 4 μs and a frequency of 10^5 pulses/s. Specimina were implanted with nitrogen ions with energy of 1.2 keV. The temperature regimes of target irradiation 450, 500, and 650 °C were determined from the readings of an isolated thermocouple installed on the reverse side of the target. The specimina were heated to the initial irradiation temperatures by an ion beam for 20 min. The time of ion-beam heating of the specimina was additional for all irradiation regimes and was not included in the total implantation time, which was 60 minutes.

The characteristic distribution of the ion current density over the beam section is shown in figure 2. In the experiments, the change in the ion current density at the maximum of the distribution, determining the temperature maximum at the center of the target, was carried out by varying the discharge current of the plasma generator.

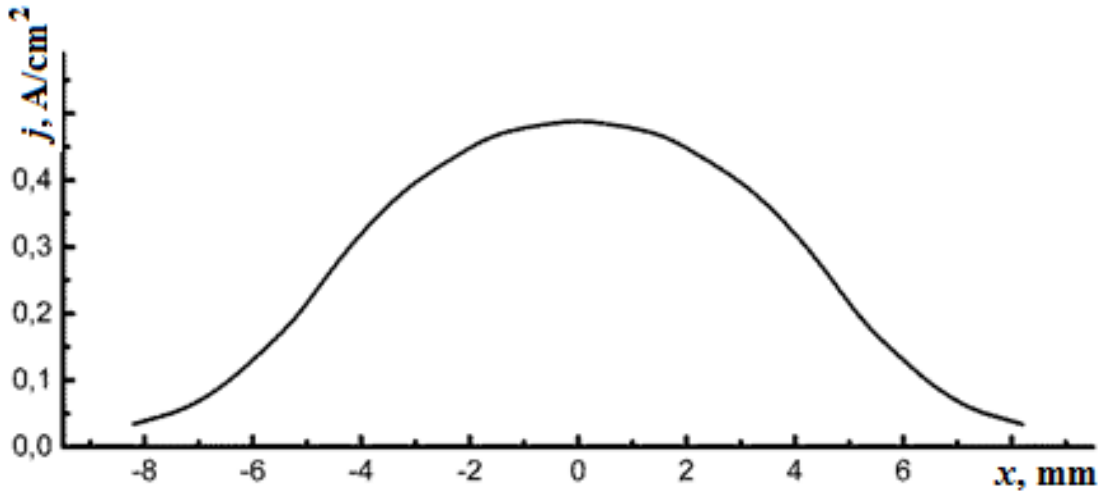

Figure 2. Ion current density distribution *j* over a cross section of a nitrogen ion beam.

Figure 3 shows the results of a numerical simulation of the temperature distribution over the irradiated composition depth for three different irradiation temperature regimes.

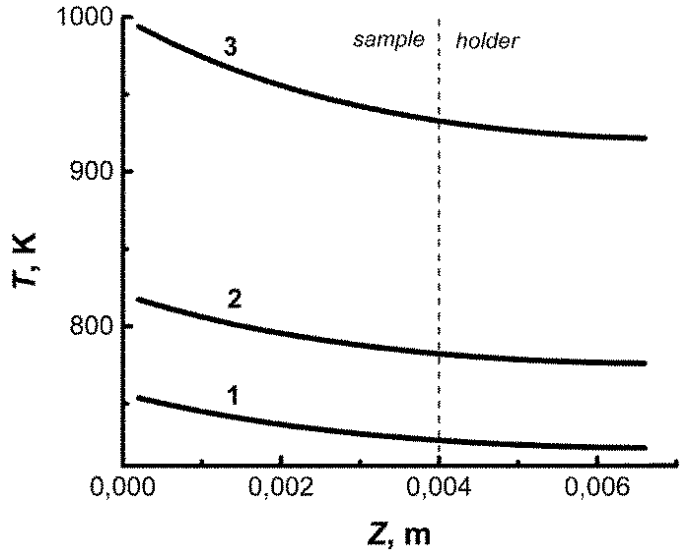

Figure 3. Temperature distribution T over the depth (Z) of the irradiated composition, along the axis $r = 0$, $t_{irr} = 60$ min, T_0: 1 – 450°C; 2 – 500°C; 3 – 650°C.

The smallest temperature gradient over the target depth occurs when exposed to an ion beam with a density of 1250 A·m^{-2}. It is about 30°C. As the ion current density increases to 1600 and 2800 A·m^{-2}, the temperature gradient over the target depth increases to 35 and 60°C, respectively.

A significant temperature gradient occurs over the target surface. This gradient is primarily due to the inhomogeneous distribution of the ion current over the beam cross section. Figure 4 shows the temperature distribution along the irradiated and reverse surfaces of the specimen in the steady state irradiation regime.

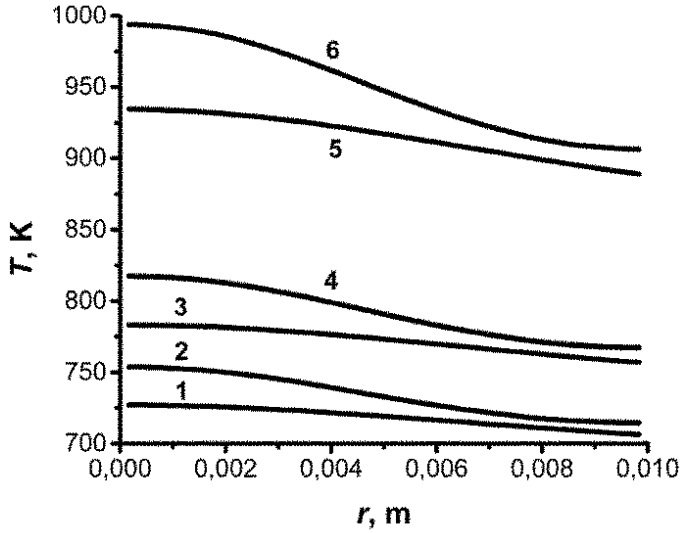

Figure 4. Temperature distribution along specimen surface ($r = 0$ – specimen cross section centre): 2, 4, 6 – irradiated specimen surface; 1, 3, 5 – lower specimen surface, $t_{irr} = 60$ min, T_0: 1, 2 – 450°C; 3, 4 – 500°C; 5, 6 – 650°C.

From the data of figure 4 it can be seen that the greatest temperature gradient over the surface of a specimen of 5140 steel occurs at the highest irradiation temperature of 650°C. It is about 90°C (curve 6 of figure 4). A slightly smaller temperature gradient occurs on the reverse side of the target. At lower ion irradiation temperatures, the gradients both on the irradiated surface (curves 4 and 2 of figure 4) and on the reverse side of the specimen should also decrease.

If the specimen temperature is measured on the reverse side of the specimen holder made of stainless steel, then, as follows from the data in figure 5, the temperature gradient along the target radius, as well as the composition depth, will increase.

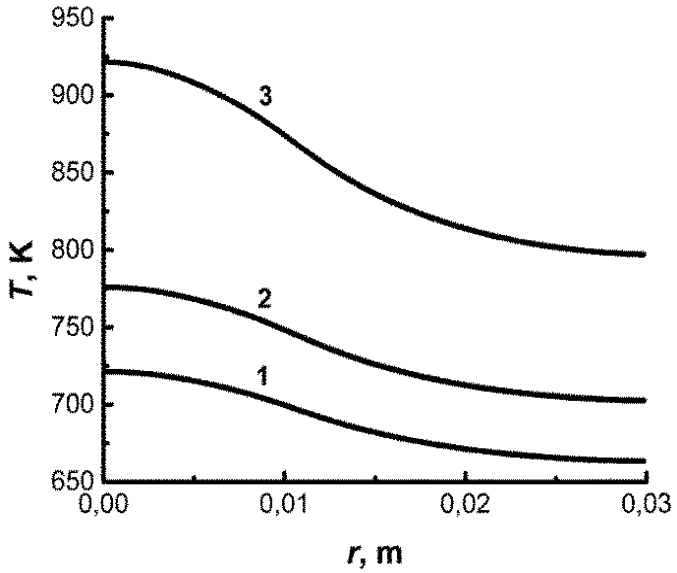

Figure 5. Temperature distribution along the back side of the holder ($r = 0$ – stainless steel holder cross section, $t_{irr} = 60$ min, T_0: 1 – 450°C; 2 – 500°C; 3 – 650°C.

It is characteristic, that with a significant increase in the ion current density, the regime of high-intensity implantation of low-energy ions can be accompanied by an increase in temperature gradients over the depth and over the surface to several hundred degrees.

Verification of the numerical calculation model of the target temperature fields during high-intensity implantation was carried out based on a comparison of data of calculations and experimental studies. Taking into account that the irradiated target during the plasma-immersion formation of the ion beam is under the high-voltage bias potential, the temperature measurement on the target back side was performed using an isolated chromel-alumel thermocouple. For a more accurate measurement of temperature and its gradients on the specimen surface, a high-temperature pulse pyrometer KLEIBER 740-LO was used.

The results of numerical simulation and experimental measurements using a thermocouple and pyrometer in the center of the target in a dynamic heating regime show satisfactory agreement (figure 6).

Thermocouple shows a slightly underestimated value at a dynamic temperature change, due to its electrical, and hence some thermal insulation. In the stationary regime with an irradiation time of more than 1000 s, there is a good agreement between the results of the numerical calculation and the thermocouple. The pyrometer data indicates a slightly lower temperature, which may be due to the time-varying reflection coefficient of the target surface due to changes in its morphology.

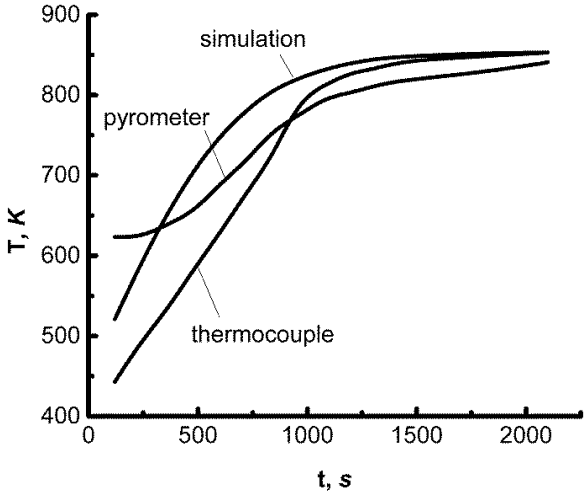

Figure 6. Results of numerical simulation and experimental measurements using a thermocouple and pyrometer in the center of the target in a dynamic heating regime.

4. Conclusion

The study of formation dynamics of the gradient temperature fields in the depth and on the surface of metal targets during implantation with high-intensity beams of gas ions and metals was carried out experimentally and by numerical simulation. There is a pretty good agreement between the data of the physical experiment and the results of numerical simulation.

In the course of the research, it was shown that the temperature gradient over the target depth increases with increasing ion current density. The greatest temperature gradient over the surface of the specimen of 5140 steel occurs at the highest irradiation temperature of 650°C.

Acknowledgments

This work was carried out with the financial support of the Russian Science Foundation (grant No. 17-19-01169).

References

[1] Poate J M, Foti G and Jacobson D C (Eds.) 2013 *Surface Modification and alloying by Laser, Ion, and Electron Beams* (Berlin: Springer)
[2] See, for instance, Proceedings of the Biennial International Conferences on the Surface Modification of Materials by Ion Beams (SMMIB) (2016) [*Surf. Coat. Technol*. **306**, Part A (2016)]; Ion Beam Modification of Materials of Materials (IBMM) (2017) [*Nucl. Instrum. Methods Phys. Res. B* **409** (2017)
[3] Brown I G, Galvin J E and MacGill R A 1985 *Applied Physics Letters* **47** 358
[4] Ryabchikov A I and Nasyrov R A 1992 *Review of Scientific Instruments* **63** 2428
[5] Bugaev S P, Nikolaev A G, Oks E M, Schanin P M and Yushkov G Yu 1994 The «TITAN» ion source *Review of Scientific Instruments* **65** 3119
[6] Gavrilov N V, Mesyats G A, Radkovski G V and Bersenev V V 1997 Development of technological sources of gas ions on the basis of hollow-cathode glow discharges *Surface and Coatings Technology* **96** 81
[7] Ryabchikov A I, Kashkarov E B, Pushilina N S, Syrtanov M S, Shevelev A E, Korneva O S, Sutygina A N and Lider A M 2018 *pplied Surface Science* **439** 106
[8] Sivin D O, Ananin P S, Ivanova A I, Lopatin I V, Korneva O S and Shevelev A E 2018 *Surface and Coatings Technology* **355** 129
[9] Ryabchikov A I, Shevelev A E, Sivin D O, Ivanova A I and Medvedev V N 2018 *Surface and Coatings Technology* **355** 123

[10] Ryabchikov A I, Kashkarov E B, Shevelev A E, Obrosov A and Sivin D O 2019 *Surface and Coatings Technology* **372** 1
[11] Ryabchikov A I, Ananin P S, Dektyarev S V, Sivin D O and Shevelev A E 2017 *Vacuum* **143** 447
[12] Ryabchikov A I, Sivin D O, Korneva O S, Lopatin I V, Ananin P S, Prokopenko N A and Akhmadeev Yu Kh 2018 *Nuclear Instruments and Methods in Physics Research, Section A: Accelerators, Spectrometers, Detectors and Associated Equipment* **906** 56
[13] Anders A 2000 *Handbook of Plasma Immersion Implantation and Deposition* (New York: John Wiley & Sons)
[14] Stepanov I B, Ryabchikov A I, Ananin P S, Dektyarev S V, Sivin D O and Verigin D A 2014 *Review of Scientific Instruments* **85** 4852219
[15] Ryabchikov A I, Sivin D O, Korneva O S, Ananin P S and Dectyarev S V 2018 *Journal of Physics: Conf. Series* **1115** 032053
[16] Ryabchikov A I, Anan'in P S, Dektyarev S V, Sivin D O and Shevelev A E 2017 *Technical Physics Letters* **43** 1051
[17] Ryabchikov A I, Sivin D O, Shevelev A É and Ananyin P S 2018 *Russian Physics Journal* **61** 1338